Received: 13 December 2024 | Revised: 19 February 2025 | Accepted: 4 June 2025
DOI: 10.1002/suco.70191

ARTICLE

fib CEB-FIP WILEY

Modeling the response of UHPC shear-critical beams: Integrating nonlinear finite element analysis and artificial neural network

Amjad Diab | **Anca Ferche**

Department of Civil, Architectural and Environmental Engineering, The University of Texas at Austin, Austin, Texas, USA

Correspondence
Amjad Diab, Department of Civil, Architectural and Environmental Engineering, The University of Texas at Austin, 301 E. Dean Keeton Street, Austin, TX 78712-C1748, USA.
Email: amjad.diab@utexas.edu

Funding information
Precast/Prestressed Concrete Institute

Abstract

An analytical framework suited for the analysis of shear-critical ultra-high performance concrete (UHPC) members is presented. The numerical methodology utilizes a nonlinear finite element analysis formulation integrated with an artificial neural network (ANN) that characterizes the UHPC tension response based on its mix design. In addition, a novel compression softening model specifically tailored for UHPC is introduced. Both of these behavioral mechanisms are necessary for a realistic assessment of the structural behavior. Special consideration is given to the influence of crack widths and the calculation of crack spacing, specific to UHPC materials. The ANN revealed that the tensile behavior of UHPC is influenced not only by the characteristics of fiber reinforcement but also by the mix design constituents. Validation studies successfully reproduced the response of published experiments on shear-critical panel specimens and beams. This study also highlights the crucial impact of UHPC direct tension characteristics on the behavior of shear-critical members. Furthermore, the influence of compression softening on the accuracy of the analytical results was found to be dependent on the magnitude of compressive stresses present.

KEYWORDS

analytical modeling, artificial neural networks, compression softening, nonlinear finite element analysis, shear, UHPC

1 | INTRODUCTION

Due to its exceptional mechanical properties and durability, ultra-high performance concrete (UHPC) has attracted significant attention as a key material shaping the future of civil infrastructure. Similar to conventional concrete, UHPC comprises inert and reactive components that undergo a hydration reaction when mixed with water and chemical admixtures.[1] In general, UHPC is characterized by prescriptive and performance requirements rather than a standardized mixture design. Typically, it incorporates a significant amount of steel fiber reinforcement, with volumetric ratios of 2% or more, while seldom including coarse aggregate. Key UHPC requirements encompass self-consolidating workability, high compressive strength (120–250 MPa), high tensile strength (5–18 MPa), and superior residual post-cracking tensile strength compared to other cementitious materials.[2] These features collectively contribute to the material's superior performance in structural applications, compared to conventional concrete, in some cases resulting in the significant reduction or elimination of conventional transverse reinforcement. As such, UHPC becomes an advantageous choice in applications such as long-span precast pretensioned elements, bridge decks, offshore platforms, nuclear power plant buildings, and blast and impact resistant structures.[3–9] In the majority of these applications, the material is subjected to significant shear forces, often without conventional shear reinforcement provided.

A critical aspect of utilizing the full potential of UHPC in various engineering applications relies on the understanding and accurate characterization of its structural response. The development of numerical procedures and constitutive models that can be used as advanced analysis tools is a key step in this process. Significant research effort was dedicated over the past few decades to the development of constitutive models for fiber reinforced concrete (FRC).[10–15] However, the applicability of these models for UHPC remains limited due to the unique characteristics of UHPC. Therefore, there is a growing need to tailor existing models or develop new ones that specifically address the mechanical behavior of UHPC.

Recent investigations have highlighted that shear-critical members depend predominantly on the UHPC direct tension behavior.[16–18] Previous studies proposed different approaches to model the tension response, ranging from micro to macro-scale models.[19–25] These models mainly focus on the interactions between fiber reinforcement and the cementitious matrix. The primary limitations of these approaches include dependency on the bond strength between the fiber reinforcement and the cementitious matrix, the need for extensive models to analyze the effect of different fiber types, in addition to the influence of the other mix design constituents on UHPC behavior. In a different study by the authors, these challenges motivated the development of an Artificial Neural Network (ANN) to predict the direct tension characteristics of UHPC based on its mix design constituents.[26]

This study presents the development of a numerical framework for analyzing shear-critical UHPC members, enhanced by the integration of an ANN to characterize the tension response of UHPC. The scope of the work is confined to UHPC shear-critical beams that do not incorporate transverse reinforcement. The reason behind this choice constitutes primarily the industry directions geared toward eliminating the conventional transverse reinforcement in UHPC beams. The numerical methodology developed in this study employs the nonlinear finite element analysis (NLFEA) software VecTor2[27] and integrates the ANN that outputs the uniaxial tensile stress–strain model of UHPC.[26] In addition, a novel compression softening model specifically tailored for UHPC is introduced. The theoretical foundation of the NLFEA framework is the Disturbed Stress Field Model,[28] utilizing a smeared hybrid rotating crack formulation. In addition to the tension and compression models customized for UHPC, the proposed approach incorporates aspects such as the crack width limit check and the crack spacing calculation. These considerations were found to enhance the accuracy of the analytical approach by accounting for the unique properties of UHPC.

To validate the accuracy of the proposed approach, a validation study was carried out, modeling the response of UHPC panels subjected to pure shear,[29] and UHPC shear-critical beams without transverse reinforcement, as documented in the literature.[4,30–33] The successful validation of the approach across diverse experimental programs underscores its applicability in capturing the behavior of shear-critical UHPC structures.

2 | MODELING OF UHPC STRUCTURAL MEMBERS

The existing modeling approaches used for UHPC are broad extensions of models developed for the response of reinforced concrete and fiber reinforced concrete, which can be classified based on their representation of cracks as either discrete crack models or smeared crack models. Discrete cracks are represented as node separations along element boundaries. This approach typically uses truss or solid elements to represent the fiber reinforcement and link elements to represent the interface between the fiber reinforcement and the concrete matrix. This methodology better suits micro- and meso-scale modeling efforts, and it is generally regarded as computationally demanding for large-scale structural assessment. Smeared crack models are generally used for most structural engineering applications. They involve modeling concrete as a quasi-continuous material with the cracks assumed to be an average deformation distributed over an area. After cracking, the concrete is treated as an orthotropic material and the effect of the cracks on the response is accounted for in terms of stiffness, strength, and energy characteristics.

Over the course of the past few decades, various smeared crack models were developed, based on the crack characteristics, including the fixed crack models,[34,35] rotating crack models,[36–39] hybrid crack models,[28,40] and micro-plane models.[12,41–44] The fixed

FIGURE 1 (a) Equilibrium conditions, (b) compatibility conditions, and (c) constitutive relations of the proposed model.

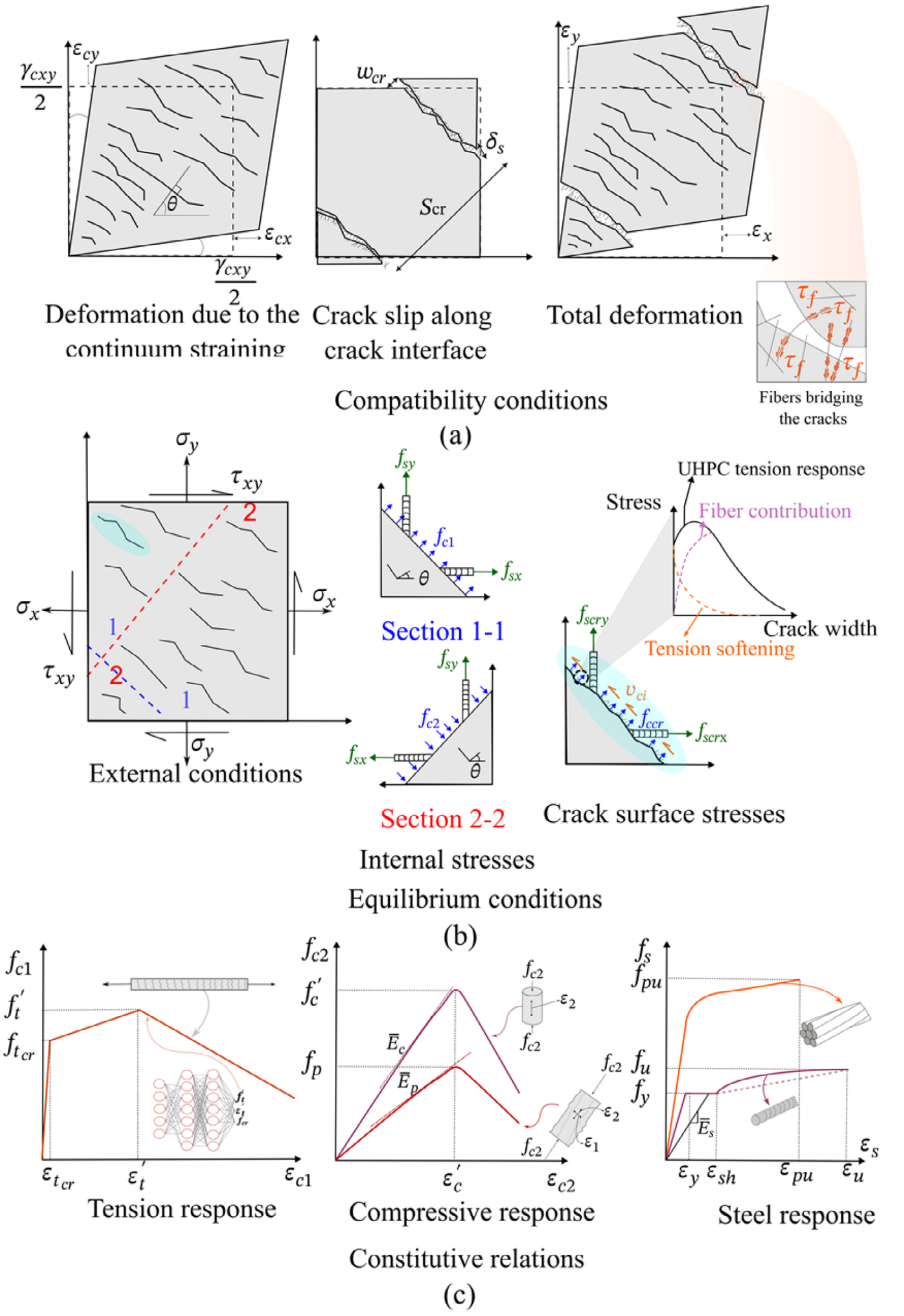

crack models maintain a constant post-cracking orientation of the crack. However, this approach can sometimes lead to stiffness overestimations, as highlighted by earlier research.[39] The rotating crack models allow for the crack orientation to evolve, due to either a change in loading conditions or a change in material stiffness. As such, these models impose a restriction that the directions of the principal strains and principal stresses remain coincident. Hybrid crack models, such as the disturbed stress field model (DSFM),[28] adopted in this study, incorporate characteristics of fixed and rotating crack models and generally allow for the principal stress and strain fields to diverge. Separate from the above are the micro-plane models, which define material behavior across multiple planes. These models capture the material responses by treating behavior across various orientations; however, it is generally accompanied by high computational costs.

This study is based on the DSFM formulation with alterations made in terms of the constitutive model formulations to account for the particularities associated with the UHPC behavior. Figure 1 provides a visual representation of the framework involving compatibility

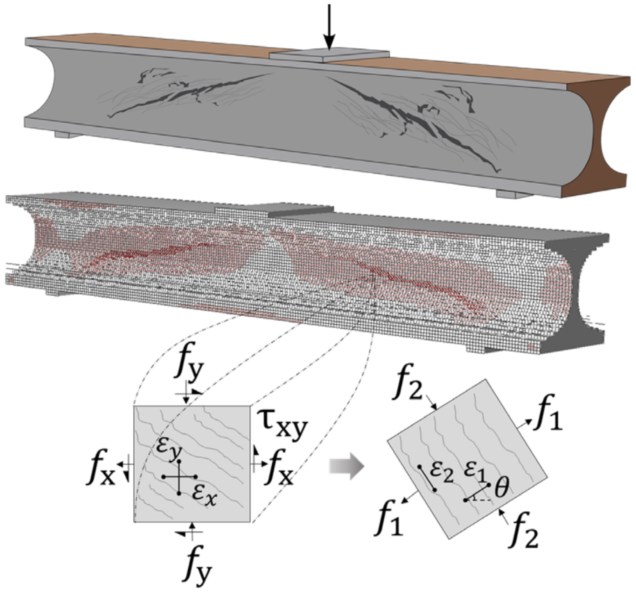

FIGURE 2 Representation of a traditional shear test of a UHPC beam and a typical finite element analysis model.

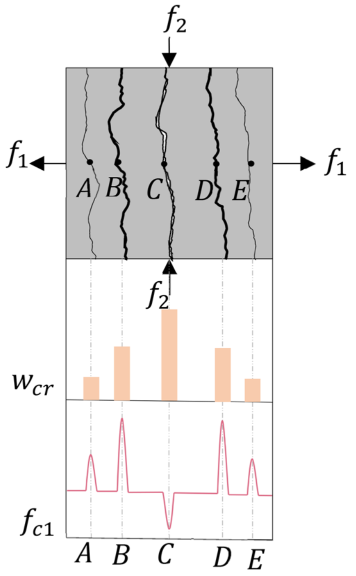

FIGURE 3 Principal tensile stress magnitude for different crack widths in UHPC elements.

conditions, equilibrium conditions, and the constitutive relations. Subsequent sections offer an in-depth discussion of each of these elements.

3 | MODEL OVERVIEW

Figure 2 illustrates a simply supported UHPC beam subjected to monotonically increasing load, representing a traditional shear test and a typical NLFEA model used to analyze its behavior. The NLFEA approach employed in this study to model such a test involves the use of plane membrane elements. This choice is informed by the predominantly two-dimensional nature of the behavior, which is particularly relevant for UHPC members such as beams or shear walls.

The membrane element depicted in Figure 2 is situated in the critical region of a traditional shear test, characterized by constant shear and varying bending moment. In this region, the beam experiences bending and shear stresses simultaneously, making it challenging to isolate and analyze shear behavior independently. As a result, developing a general theory for shear behavior based solely on beam testing is challenging. As such, in this study, the initial effort was geared toward examining and characterizing the response of such a UHPC membrane element subjected to pure shear stresses, to gain insight into fundamental aspects of behavior, followed by the analysis of beam specimens.

Illustrated in Figure 3, is the UHPC element rotated to align with the principal stress directions, showing the principal tensile direction, f_1, and the principal compressive direction, f_2. In contrast with conventional concrete, non-zero tensile stresses are present at the crack's location due to the fiber reinforcement bridging the cracks. It is important to note that, depending on the characteristics of UHPC tensile response, the magnitude of the average tensile stresses may increase post-cracking, due to the strain-hardening effect, followed by a gradual decrease as the crack width, w_{cr}, increases and the fibers pull out or rupture. If conventional steel reinforcing bars are provided, they will also contribute to the load-carrying mechanism at the crack locations, as explained elsewhere.[27,28]

3.1 | Compatibility conditions

Shown in Figure 1a is an element experiencing deformations due to continuum straining and slip along the crack interfaces. Figure 1a also highlights the fiber reinforcement bridging the cracks and the bond stresses (τ_f) acting along the interface between the fibers and the cementitious matrix. Consistent with the DSFM formulation,[28] the continuum straining is linked to the average constitutive response of the UHPC, and the slip component is the result of rigid body movement along the crack. The total strains, containing both components, are denoted as $[\varepsilon] = \left[\varepsilon_{\mathrm{x}}, \varepsilon_{\mathrm{y}}, \gamma_{\mathrm{xy}}\right]$; the net strains due to continuum straining are denoted as $[\varepsilon_{\mathrm{c}}] = \left[\varepsilon_{\mathrm{cx}}, \varepsilon_{\mathrm{cy}}, \gamma_{\mathrm{cxy}}\right]$, while the slip strain is denoted as $[\varepsilon^{\mathrm{s}}] = \left[\varepsilon^{\mathrm{s}}_{\mathrm{x}}, \varepsilon^{\mathrm{s}}_{y}, \gamma^{s}_{xy}\right]$.

Standard transformations are employed to determine the principal strains and their orientations.

As shown in Figure 1a, the cracks are considered to be perpendicular to the direction of the net principal tensile strain, θ, having an average width, w_{cr}, and spacing, s_{cr}. The slip along the crack interfaces is denoted as δ_s. As such, the average shear slip strain is calculated as $\gamma_s = \delta_s / s_{cr}$, where $\varepsilon_x^s = -\gamma_s/2\sin(2\theta)$, $\varepsilon_y^s = \gamma_s/2\sin(2\theta)$, and $\gamma_{xy}^s = \gamma_s/2\cos(2\theta)$, according to the DSFM.[28] Additionally, the formulation takes into consideration strains due to elastic offsets, $\left[\varepsilon_c^o\right]$ such as thermal expansion, Poisson's effects, and plastic offsets, $\left[\varepsilon_c^p\right]$, due to cyclic loading, as described elsewhere.[28,45] Therefore, the total strains are calculated as:

$$[\varepsilon] = [\varepsilon_c] + \left[\varepsilon_c^s\right] + \left[\varepsilon_c^o\right] + \left[\varepsilon_c^p\right] \tag{1}$$

Perfect bond is assumed between the concrete and the conventional steel reinforcement. The total strain of the conventional steel reinforcement is calculated as:

$$[\varepsilon] = [\varepsilon_s] + \left[\varepsilon_s^o\right] + \left[\varepsilon_s^p\right] \tag{2}$$

where $[\varepsilon_s]$ is the net steel strain, $\left[\varepsilon_s^o\right]$ and $\left[\varepsilon_s^p\right]$ are the elastic and plastic strain offsets of steel reinforcement components.

The average crack spacing, s_{cr}, is calculated as:

$$s_{cr} = 0.75 l_f \tag{3}$$

where l_f is the average length of the fiber reinforcement in the UHPC mix. This value was estimated based on the average crack spacing values observed in previous experimental and analytical studies.[46–48]

The average crack width is evaluated as the product between the average principal tensile strain and the average crack spacing, as:

$$w_{cr} = s_{cr}.\varepsilon_{c1} = 0.75 l_f.\varepsilon_{c1} \tag{4}$$

The slip along the crack interfaces, δ_s, was evaluated according to the procedure elaborated in Wong et al.,[27] based on the Walraven model,[49] as:

$$\delta_s = \frac{v_{ci} + v_{co}}{1.8\, w_{cr}{}^{-0.8} + \left(0.234 w_{cr}{}^{-0.707} - 0.2\right) f_{cc}} \le 2 w_{cr} \tag{5}$$

where v_{ci} is the shear stress acting along the crack interfaces, evaluated from equilibrium conditions as shown in the following section, $v_{co} = f_{cc}/30$ is an initial offset in the crack shear-slip relationship, and f_{cc} is the cube compressive strength. The conversion factors for the compressive strength are based on previous studies on the compressive strength behavior of UHPC specimens.[50–52] A 100 × 100 mm cube was adopted as the reference compressive strength for this study.

3.2 | Equilibrium conditions

Equilibrium conditions are examined from two distinct perspectives: the average stresses distributed across the element continuum, and the localized conditions at the crack interfaces, similar to the approach of the modified compression field theory (MCFT) and the DSFM.[28,39] The equilibrium criteria, considering both the average and localized conditions, are graphically depicted in Figure 1b.

The fiber reinforcement is considered smeared in UHPC elements. Hence, non-zero UHPC average tensile stresses are included in the formulation after cracking, regardless of the conventional steel reinforcement configuration. The element equilibrium equation is:

$$[\sigma] = [D_c][\varepsilon_c] + \sum_{i=1}^{n} [D_s]_i [\varepsilon_s]_i \tag{6}$$

where $[D_c]$ and $[D_s]_i$ are the global concrete and conventional reinforcement stiffness matrices, n is the number of conventional reinforcement components, and $[\varepsilon_c]$ and $[\varepsilon_s]_i$ are the net strains in concrete and conventional reinforcement, respectively.[27]

In the MCFT and DSFM formulations, the crack interfaces are considered as planes of weakness in the continuum, as such, equilibrium conditions are also evaluated at the crack location. The magnitude of the tensile stresses transmitted across the crack is governed by the yield strength of the conventional steel reinforcement and the post-cracking tensile response of UHPC. The additional strain at crack locations ($\Delta\varepsilon_{1cr}$) is iteratively calculated to estimate the total strain at crack location (ε_{1cr}) as:

$$\varepsilon_{1cr} = \varepsilon_1 + \Delta\varepsilon_{1cr} \tag{7}$$

The local strain (ε_{scri}) and stress (f_{scri}) in the steel reinforcement at the location of the crack are calculated as:

$$\varepsilon_{scri} = \varepsilon_{si} + \Delta\varepsilon_{1cr}.\cos^2\theta_{ni} \tag{8}$$

$$f_{scri} = E_s.\varepsilon_{scri} \le f_{yi} \tag{9}$$

where θ_{ni} is the angle between the "*i*" reinforcement component and the principal tensile stress direction as shown in Figure 1b. The equilibrium conditions at the crack interfaces are expressed as:

$$f_{c1} = \sum \rho_i (f_{scri} - f_{si}) \cos^2\theta_{ni} \tag{10}$$

After iteratively solving the set of Equations (7)–(9) to find $\Delta\varepsilon_{1cr}$, the shear stress along the crack is calculated as:

$$v_{ci} = \sum \rho_i (f_{scri} - f_{si}) \cos\theta_{ni} \sin\theta_{ni} \tag{11}$$

3.3 | Constitutive relations

3.3.1 | Compression behavior

The compression stress–strain model proposed by Hoshikuma et al.[53] was employed for the pre-peak response of UHPC elements. The equation for the pre-peak compressive response model stress is given by:

$$f_{ci} = E_c \varepsilon_{ci} \left(1 - \frac{1}{n}\left(\frac{\varepsilon_{ci}}{\varepsilon_p}\right)^{n-1}\right) \quad \text{for } \varepsilon_p < \varepsilon_{ci} < 0 \tag{12}$$

$$n = \frac{E_c}{E_c - E_{sec}} \tag{13}$$

$$E_{sec} = \frac{f_p}{|\varepsilon_p|} \tag{14}$$

where f_{ci} is the concrete compressive stress, ε_{ci} is the concrete principal compressive strain, f_p and ε_p represent the UHPC peak compressive strength and strain at peak compressive strength respectively. The parameter n expresses the deviation from linear behavior in terms of the initial tangent stiffness E_c, and secant stiffness E_{sec}.

Previous experimental studies noted that the confined pre-peak behavior of UHPC reaches up to 1.1–1.2 times the uniaxially loaded UHPC cylinders under compression.[54] As such, Kupfer's model for strength enhancement due to confinement was adopted in this study.[55]

The post-peak response was modeled as:

$$f_{ci} = -\left[f_p + E_{des}(\varepsilon_{ci} - \varepsilon_p)\right] \le -0.2 f_p \text{for } \varepsilon_{ci} < \varepsilon_p < 0 \tag{15}$$

$$E_{des} = \frac{11.2 {f_c'}^2}{\left(\frac{f_{lat}}{2}\right)} \le 0.5 E_c \tag{16}$$

$$f_{lat} = f_{c1} + f_{c2} + f_{c3} - f_{ci} \le 0 \tag{17}$$

where E_{des} represents the post-peak tangential stiffness, f_{lat} is the summation of principal stresses acting transversely to the compressive direction. Further details can be found elsewhere.[27]

3.3.2 | Compression softening behavior

In numerous practical applications, especially shear-critical members, the UHPC material will be under a predominantly biaxial stress state, involving coexisting principal compressive and tensile stresses. The transverse tensile stresses were found to reduce the compressive strength of UHPC elements, compared to UHPC under uniaxial compression, therefore, resulting in a compression softening mechanism similar in nature to the compression softening observed in conventional concrete.[17,32,54,56,57] To represent numerically the compression softening mechanism, the uniaxial compressive strength is multiplied by the compression softening factor β to obtain the maximum compressive strength of cracked UHPC, f_p, as such:

$$f_p = \beta \cdot f_c' \tag{18}$$

Experimental observations indicate that the strain at peak stress of UHPC is similar for uniaxial compression and biaxial tension-compression loading.[58] As a result, in this study, β is only applied to the compressive strength, f_c', and not to the strain at peak compressive strength. The model was developed based on recent experimental studies examining the response of cracked UHPC members which are summarized in Table 1 including the number of tested specimens, test type, member dimensions, fiber type and percentage, and the longitudinal and transverse reinforcement ratios ρ_l, and ρ_v respectively.

The experimental results of the studies summarized in Table 1 were categorized in terms of the fiber reinforcement content in Figure 4a. The results indicate that incorporating fiber reinforcement at even low percentages, such as 1.0%, reduces the severity of compression softening when compared to UHPC panels without fiber reinforcement. No clear trend was discerned on the influence of fiber content (within 1.0% and 2.5% range) on compression softening. This indicates that the main parameters governing the compression softening response of UHPC members are the transverse tensile strains and the presence of fiber reinforcement above a 1.0% fiber content.

TABLE 1 Summary of the experimental programs on the cracked response of UHPC members.

	Fehling et al.[56]	Lee et al.[54]	Leutbecher[49]	Liu et al.[58]	Yap[29]	El-Helou and Graybeal[32]
No. of specimens	47	30	31	11	5	6
Test type	a	a	a	a	b	c
Length (mm)	500	240	500	940	1626	9750–11,580
Height (mm)	350	190	350	940	1626	889–1092
Thickness (mm)	70	90	70	80	200	76–102
Fiber type	S.F[a]	S.F	S.F	S.F	S.F & H.F[b]	S.F
Fiber %	1.0%	0.0%–1.5%	1.0%	2.5%	2.0%	2.0%
ρ_l[c]	0.9%	4.2%	1.6%	0.0%	0.0%–2.6%	1.6%–2.2%
ρ_v[d]	1.6%	2.0%	0.9%	0.0%	0.0%–0.9%	0.0%–1.3%
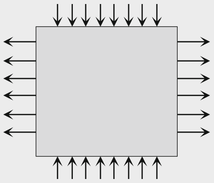		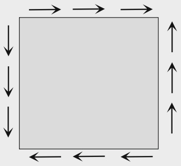		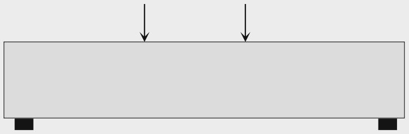		
(a) Biaxial test on panel elements with constant tensile load and increasing compression load.		(b) Pure shear test on panel elements.		(c) Shear-critical beam test.		

[a] S.F: Straight fibers.

[b] H.F: Hooked fibers.

[c] ρ_l: longitudinal reinforcement ratio.

[d] ρ_v: transverse reinforcement ratio.

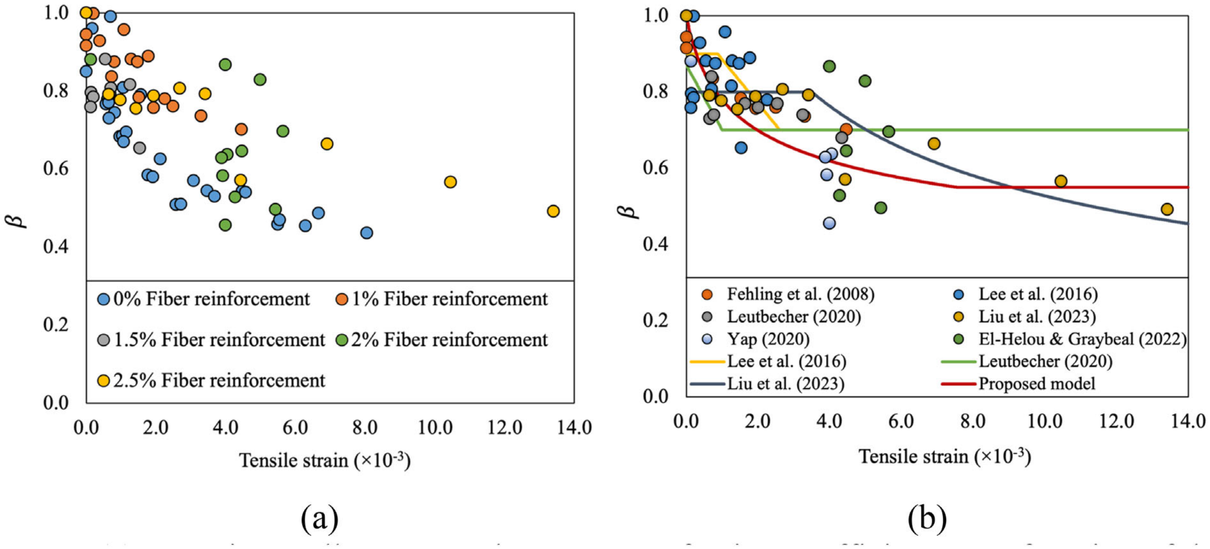

FIGURE 4 (a) Experimentally measured compression softening coefficients as a function of the fiber reinforcement content. (b) Summary of the experimentally measured compression softening coefficients, proposed, and existing compression softening models versus the transverse tensile strain.

Shown in Figure 4b and Table 2 are the comparison between the experimentally measured data and the proposed compression softening model, as well as existing compression softening models. The accuracy of the compression softening models in capturing the experimentally observed results was investigated and it is summarized in Table 2, including the ratio of experimental to theoretical compression softening coefficients and the coefficient of variation percentage (COV %). The results show that the proposed model has a superior accuracy, compared to the existing models.

TABLE 2 Performance of different UHPC compression softening models.

		$\beta_{\text{experimental}}/\beta_{\text{theoretical}}$	
	Compression softening model	**Mean**	**COV%**
Ueda et al.[66]	$\beta_{\text{Ueda}}=\frac{1}{0.8+0.6\,(1000\varepsilon_1+0.2)^{0.39}}$	1.29	22.7
Lee et al.[54]	$\beta_{\text{Lee}}=0.7<1-115\varepsilon_1<0.9$	1.14	16.2
Leutbecher[57]	$\beta_{\text{Leautbecher}}=0.87-170\varepsilon_1$	1.04	19.9
Liu et al.[58]	$\beta_{\text{Liu}}=\begin{cases}0.8 & ,\varepsilon_1\leq 3.5\\ \frac{0.8}{\sqrt{1+200\,(\varepsilon_1-3.5)}} & ,\varepsilon_1>3.5\end{cases}$	1.10	18.6
El-Helou and Graybeal[32]	$\beta_{\text{El-Helou\&Graybeal}}=0.5$	0.72	22.7
Proposed model	$\beta=\frac{1}{(1+2500\varepsilon_1)^{0.20}}\geq 0.55$	1.02	14.3

For all of the experimental studies investigated herein, the ratios of the compressive strength under biaxial tension-compression loading to the uniaxial compressive strength, β (compression softening parameter), versus the applied tensile strains are presented in Figure 4b. Unsurprisingly, the results show that compression softening is more pronounced as the transverse tensile strains increase. It is important to note that due to the nature of the tests, the panels tested under pure shear by Yap,[29] which had dissimilar reinforcement amounts in the x- and y-directions, involved a certain level of crack rotation and therefore, slip along the cracks. A similar phenomenon is expected to have developed for the shear-critical beams tested by El-Helou and Graybeal.[32] In these cases, the experimentally observed softening is a combination of both compression softening and crack slip. The latter occurs when the relative displacement along the crack interfaces reduces the effective stress transfer, further exacerbating the softening effect. This is the primary reason for the data points for the Yap[29] and El-Helou and Graybeal[32] specimens to tend to fall below the others in Figure 4b.

3.3.3 | Tension behavior

Significant research effort was dedicated recently to characterize the tensile response of UHPC elements, resulting in the emergence of numerous models. These models can be classified based on the scale of analysis, distinguishing between micro-scale and macro-scale models. The micro-scale approaches model the geometric and physical properties of the fiber reinforcement and account for the concrete matrix–fiber interactions.[14,15,59,60] The micro-scale models are generally computationally costly because of the nature of the analysis and are not readily suitable for structural-level assessment. The macro-scale models developed for structural-level analysis are largely based on direct tension tests, splitting tension tests, and flexural tests, as the most commonly used testing methods for characterizing the tensile behavior of UHPC. The experimentally measured tensile strength values exhibit variations influenced by the tensile stress distribution and corresponding boundary conditions in various tests. Notably, the direct tension test stands out for its advantageous features, offering a uniform stress condition and the capability to capture the complete stress–strain response both before and after cracking.

It is also worthy to note that the experimentally measured tension stress–strain response of UHPC varies based on the test method and mix composition, as illustrated in Figure 5. Specifically, Figure 5a shows typical responses of UHPC specimens subjected to direct tension tests, encompassing strain softening, elastic–plastic, and strain stiffening behavior. The manifestation of these behaviors is intrinsically connected to the UHPC mix design, the physical attributes of the fiber reinforcement within the mix, and the strain rate of the applied load. Notably, for the same mix design, the response characteristics can vary between direct tension and bending tests, as shown in Figure 5b.

The constitutive model for the tension response is particularly influential when modeling the behavior of shear-critical elements, given the strong correlation between their overall structural response and the tensile characteristics of UHPC.[32] This served as the motivation for the development of an ANN algorithm which can map the interconnected relations between the constituents of UHPC mix and their corresponding effect on the tension behavior.[26] Figure 6 illustrates the components of the model developed to calculate the cracking stress, f_{tcr}, ultimate tensile strength, f'_t, and the strain at the ultimate tensile strength ε'_t.[26]

The model was developed using a database containing 490 experimental data points from 19 different experimental programs with direct tensile strength,

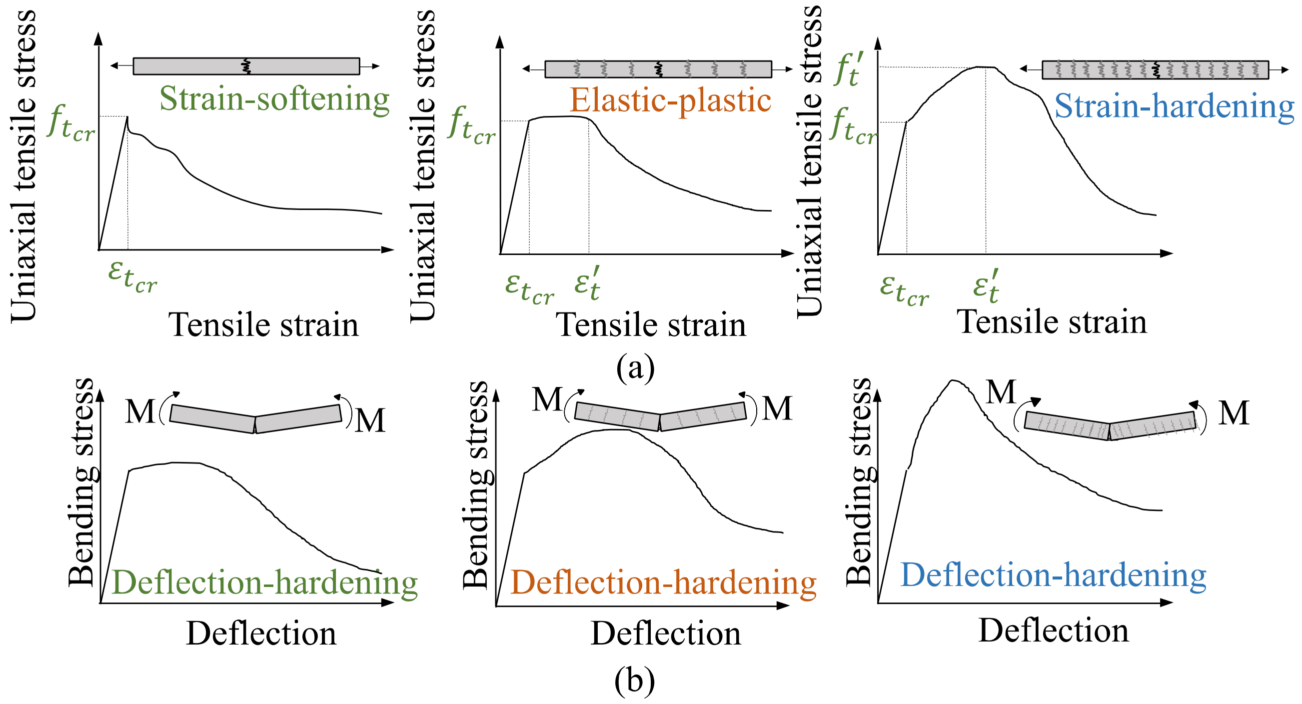

FIGURE 5 Typical tension behavioral responses of UHPC under (a) direct tension test and (b) bending test.

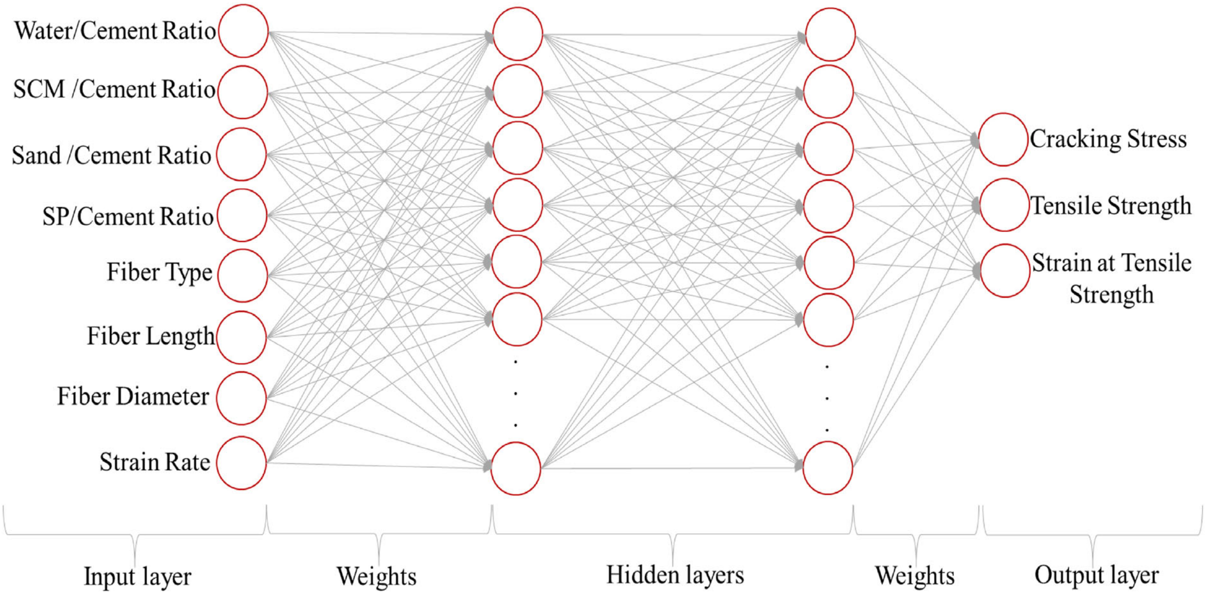

FIGURE 6 Schematic of the ANN employed.[26]

cracking stress, and the strain at the tensile strength of UHPC mixes. These values were obtained from tests conducted on UHPC specimens that were tested under uniaxial tension at different strain rates. More details on the compiled database can be found in the online repository created by the authors.[61] The ANN was trained using 80% of the data points in the database, the rest were used for testing the accuracy of the algorithm. The ANN was composed of one input layer, two hidden layers, and one output layer. ReLU was selected as the activation function for the neurons in the developed algorithm due as it had the minimum mean squared error (MSE) in the testing phase as shown in Figure 7a, and the number of neurons in the first and second hidden layers were selected as 100 and 120, respectively as they had the lowest MSE error as

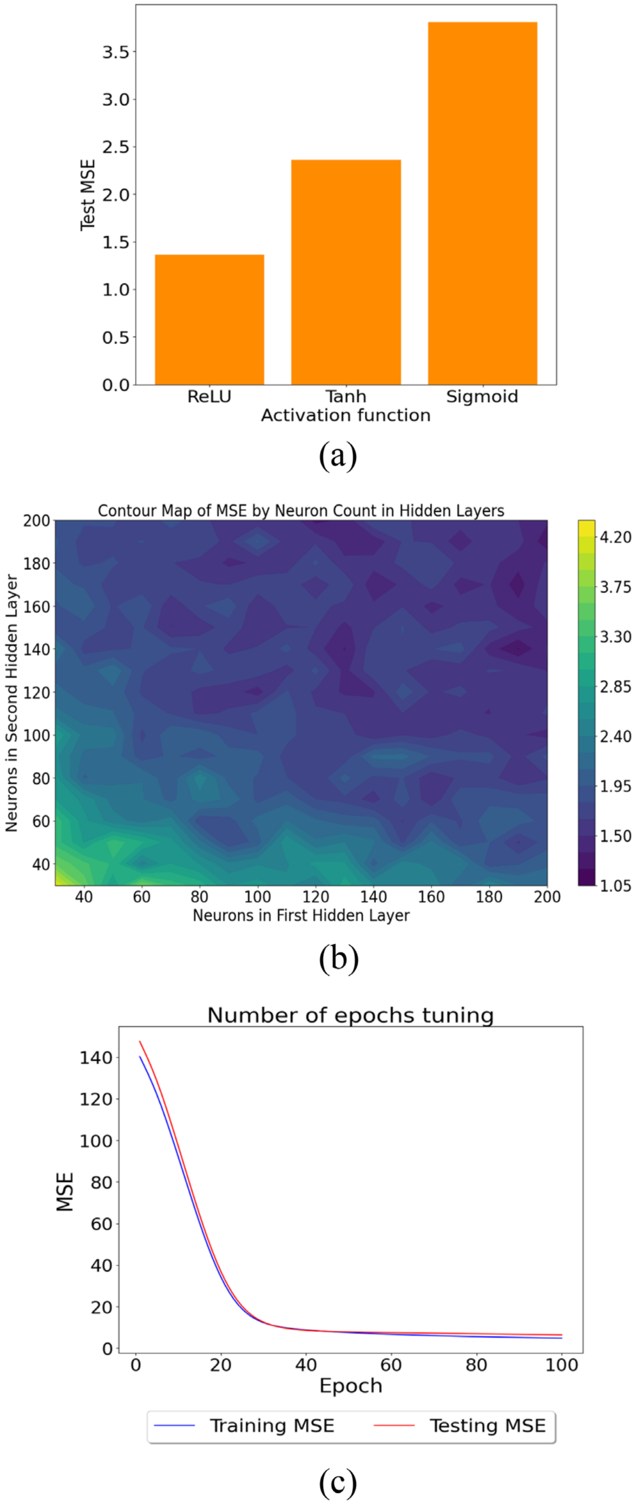

(a)

(b)

(c)

FIGURE 7 ANN parameter tuning in terms of (a) activation function, (b) number of neurons in the first and second layer, and (c) number of epochs for training.

shown in Figure 7b. The MSE error values at different iterations or epochs are provided in Figure 7c.

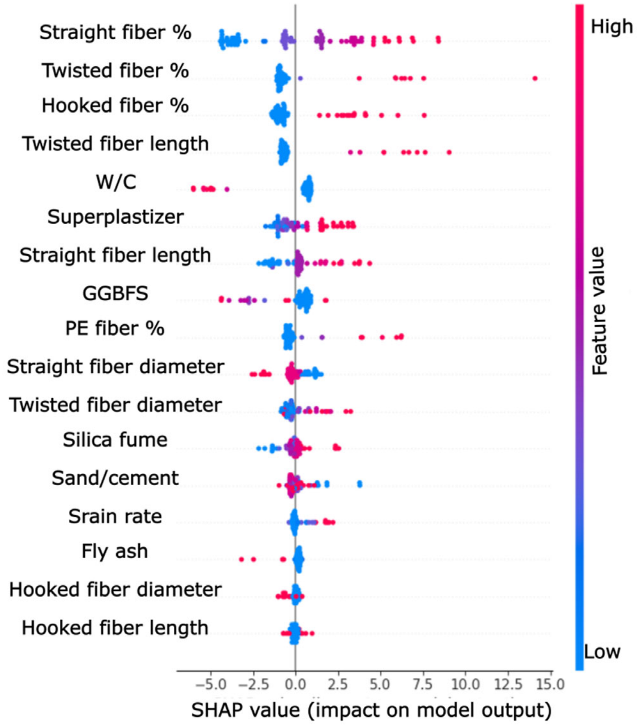

FIGURE 8 SHAP analysis results for explaining the weight of each input on the developed ANN outputs.

The results showed good accuracy in estimating the tensile properties of UHPC mixes with an overall R^2 value of 0.92 for the tensile strength of UHPC mixes. The model also showed similar accuracies in estimating the cracking tensile stress and the strain at the tensile strength. In the work presented in this paper, the ANN was integrated within the proposed framework to characterize the average tension response of the UHPC.

In this study, SHapley Additive exPlanations (SHAP) was used as the interpretation tool for the proposed ANN. SHAP quantifies the contribution of each input parameter (either a positive or negative contribution) to the output values, therefore enhancing the transparency and comprehensibility of the ANN. It can not only facilitate a deeper understanding of how the decision process is derived but also empower developers to identify and rectify potential biases within the model. The results of the developed SHAP analysis are provided in Figure 8.

The analysis results show the relative importance of the various input parameters on the direct tension strength of UHPC, ranked by their influence from top to bottom. The results show that, although the fiber reinforcement percentage has the highest weight on the direct tension strength, the other input parameters, such as the W/C ratio, supplementary cementitious materials (SCM) content, and sand to cement content, also have an influence on the direct tension strength that must be considered in UHPC tension models.

The tensile behavior of UHPC exhibits notable differences compared to conventional concrete. These distinctions include higher cracking stresses, enhanced post-cracking peak tensile strength, and greater strain magnitude at peak tensile strength, as illustrated in Figure 1c. To accurately characterize this distinct tensile behavior of UHPC, a trilinear function is employed as follows:

$$f_1 = \begin{cases} E_c \varepsilon_{c1} & \varepsilon_{c1} \leq \varepsilon_{t_{cr}} \\ f_{t_{cr}} + \dfrac{f'_t - f_{t_{cr}}}{\varepsilon'_t - \varepsilon_{t_{cr}}}\left(\varepsilon_{c1} - \varepsilon_{t_{cr}}\right) & \varepsilon_{t_{cr}} < \varepsilon_{c1} \leq \varepsilon'_t \\ f'_t - \dfrac{f'_t - f_{t_{cr}}}{\varepsilon'_t - \varepsilon_{t_{cr}}}\left(\varepsilon_{c1} - \varepsilon'_t\right) & \varepsilon_{c1} > \varepsilon'_t \end{cases} \tag{19}$$

Where $\varepsilon_{t_{cr}}$ is the cracking tensile strain, $f_{t_{cr}}$ is the cracking tensile stress, f'_t is the peak tensile strength, and ε'_t is the tensile strain at peak tensile strength. In the work presented herein, when available, these values were obtained from the direct tension test results. When tensile properties from direct tension tests were not reported for UHPC, they were obtained employing the ANN model.

3.3.4 | Crack width check

UHPC can experience significant straining at crack locations. Therefore, a crack width limit is used to reflect the inability of the UHPC material to transmit compressive stresses across large crack widths. This is because the compressive softening values in UHPC do not impose limitations under conditions of increased tensile strains. Hence, the crack width limit check serves as a critical measure to ensure modeling accuracy under varying stress conditions. The crack width check is implemented by reducing the average compressive stress computed from the stress–strain response f_{c2}, by a crack coefficient β_{cr} as:

$$f_{c2} = \beta_{cr} f_{c2} \tag{20}$$

$$\beta_{cr} = \begin{cases} 1 & \text{for}\, w < w_l \\ 1 - \dfrac{(w - w_l)}{3} \geq 0 & \text{for}\, w > w_l \end{cases} \tag{21}$$

where w is the crack width and w_l is the crack width limit in millimeters. In this work, the limiting crack width was set to 5 mm. This limit was chosen based on average crack widths reported in experimental investigations focused on the behavior of shear-critical UHPC beams.[16,62,63]

3.3.5 | Conventional reinforcement constitutive models

In this study, the model used to represent the behavior of non-prestressed steel reinforcement is composed of three phases: an initial linear-elastic response phase, followed by a yield plateau and a nonlinear strain-hardening phase, continuing up to the point of rupture.[27] While the constitutive model adopted for the prestressing steel is a Ramberg-Osgood function, as shown in Figure 1c.[27] The stress–strain response for non-prestressed reinforcement and prestressing steel are illustrated in Figure 1c. The constitutive model adopted for the prestressing steel is a Ramberg-Osgood function, as shown in Figure 1c.[27]

4 | MODEL VALIDATION

The validation of the proposed framework for modeling the response of UHPC members involved a three-phased analysis procedure. The analysis procedure was structured as follows:

1. First Phase: This initial stage focused on modeling the behavior of UHPC panels and served to establish a baseline for the model's accuracy in simulating the pure shear behavior of UHPC panels.
2. Second Phase: In this phase, the model's precision was further evaluated to validate its capability to model the response UHPC members for which experimental data was available on the tensile properties of UHPC as obtained from direct tension tests. The goal was to verify the model's accuracy in modeling large-scale UHPC members.
3. Third Phase: The third phase of the analysis involved testing the model's effectiveness in simulating UHPC members behavior using the calculated tensile properties obtained from the ANN previously developed.[26] This phase aimed to validate the integration of ANN within the NLFEA framework and its accuracy in reflecting the behavior of UHPC members.

Each phase of this procedure played a crucial role in validating the developed model, ensuring its robustness and reliability in simulating the complex behavior of UHPC members under various conditions. The transition from experimental to predictive results helped in establishing the model's applicability in practical scenarios.

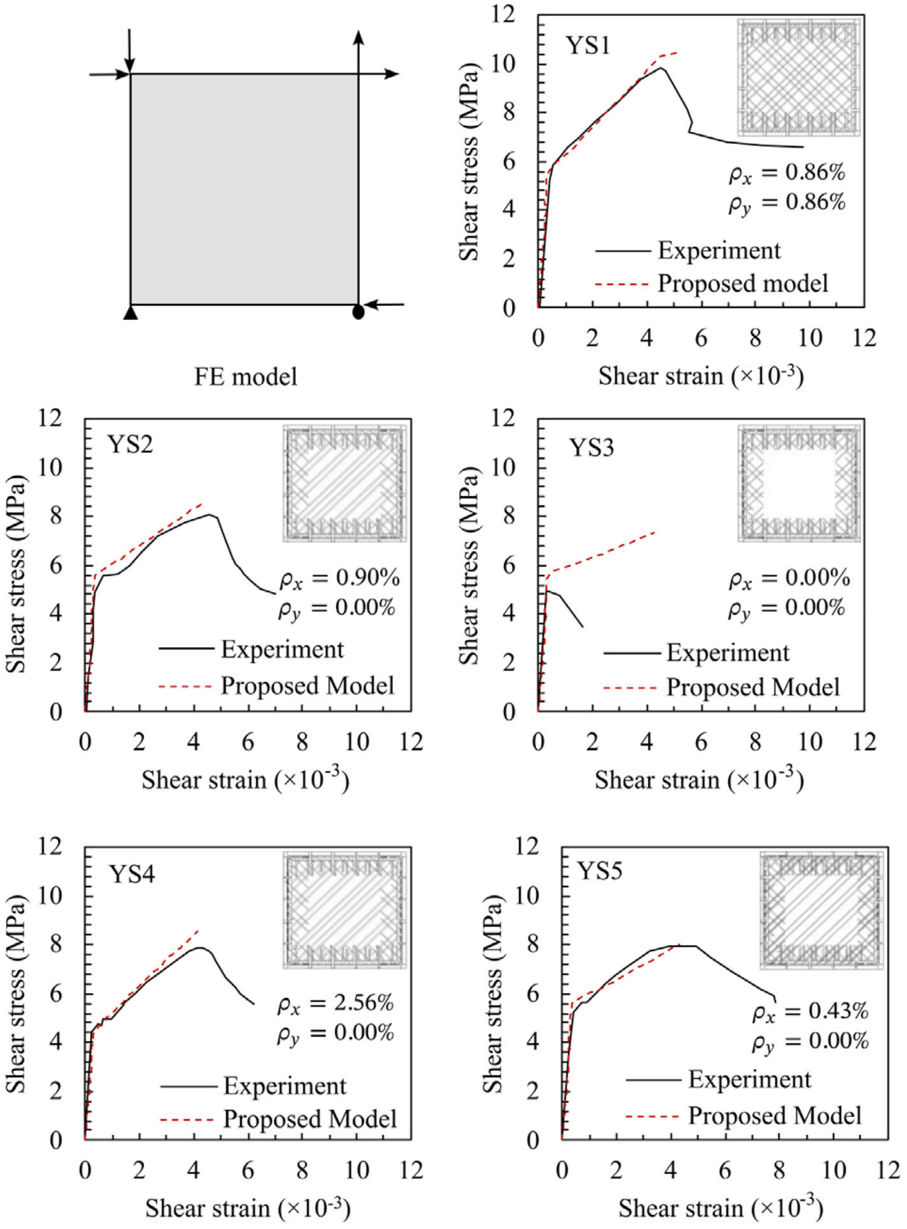

FIGURE 9 Modeling illustration and experimental versus analytical results for the UHPC panels.

4.1 | Panel specimens—Phase I

The initial phase of the validation study focused on modeling the response of UHPC panel specimens, tested by.[29] Details of this experimental program were summarized in the previous section. The finite element model consisted of a plane stress rectangular element, with the pure shear loading condition applied in a force-controlled manner. The test conditions resulted in a uniform shear stress state across the elements; therefore, it was deemed appropriate to model the specimens using a single four-nodded plane stress element. The reinforcement was modeled as smeared reinforcement with the mechanical properties measured from coupon tests reported in the experimental program.[29] The boundary conditions were representative of the test setup, consisting of a pin and a roller, as shown in Figure 9.

Table 3 provides the mechanical characteristics of the UHPC material. The compressive strength of the UHPC was determined using cylinder samples. Additionally, the tensile cracking stress and the peak tensile strength were obtained from dog-bone test results. The authors employed the previously developed ANN[26] to calculate the strain at peak tensile strength of the UHPC.

The comparison between the analytical and experimental results is shown in Figure 9 in terms of shear stress versus shear strain. A good agreement can be observed for four out of the five panels analyzed. For the

TABLE 3 Properties of the UHPC panels.[29]

Specimen	f'_c MPa	f'_t MPa	f_{cr} MPa	ε'^{a}_t $\times10^{-3}$	E_c GPa	ρ_x %	ρ_y %
YS1	171.5	7.4	5.4	4.1	49.6	0.86	0.86
YS2	167.5	7.4	5.4	4.1	46.4	0.90	0.00
YS3	164.2	7.4	5.4	4.1	48.0	0.00	0.00
YS4	157.0	6.2	4.3	4.1	47.1	2.56	0.00
YS5	160.3	7.4	5.4	4.1	46.6	0.43	0.00

Note: f'_c: UHPC compressive strength. f'_t: UHPC tensile strength. f_{cr}: UHPC cracking stress. ε'^{a}_t: UHPC strain at peak tensile strength (values were calculated using the developed ANN model). E_c: UHPC Young's modulus of elasticity. ρ_x: conventional steel reinforcement ratio in the *x*-direction. ρ_y: conventional steel reinforcement ratio in the *y*-direction.

TABLE 4 Properties of the UHPC specimens.[32]

ID	f'_c MPa	f'_t MPa	f_{cr} MPa	ε'_t $\times10^{-3}$	b_w mm	H mm	$A_{p_{bot}}$ mm^2	a/d -
H-P1	137.0	11.3	10.5	3.7	76	889	4552.8	3.5
J-P1	158.0	8.6	7.9	5.2	76	889	4552.8	3.5
J-P1S	152.0	9.3	8.9	4.4	102	889	3414.6	3.5
H-P2	140.0	10.7	10.8	3.2	76	889	4552.8	3.5
H-P3	158.0	10.9	10.6	2.8	76	1092	4552.8	3.5

Note: f'_c: UHPC compressive strength; f'_t: UHPC tensile strength; f_{cr}: UHPC cracking stress; ε'^{a}_t: UHPC strain at peak tensile; b_w: web width; H: height; $A_{p_{bot}}$: prestressed steel reinforcement area; a/d: shear-span to depth ratio.

YS3 panel, however, discrepancies between the calculated and the experimentally measured responses are evident. The panel did not develop significant post-cracking resistance experimentally, compared to the NLFEA results. Potential sources for the observed discrepancy include fiber orientation and uniformity of the applied stress. This suggests that UHPC members without conventional reinforcement may not manifest the expected strain hardening behavior, emphasizing the necessity for careful evaluation in the design and analysis of such members.

4.2 | Beam specimens—Phase II

The second phase of the validation process involved modeling UHPC beam specimens as tested by El-Helou and Graybeal.[32] This stage aimed to validate the integration of mechanical properties obtained from direct tension tests within the average constitutive model for the UHPC in tension for modeling the behavior of UHPC beams. Additionally, it served to verify the effectiveness of the compression softening model in accurately representing the biaxial stress state of shear-critical UHPC beams.

The experimental program involved the testing to failure of six shear-critical bulb-tee pretensioned bridge girder specimens. The beams were made with two different UHPC mix that were imported from different mix plants with different mechanical properties of UHPC as reported in Table 4. The mixes were denoted as mix "H" and "J", both mix designs included 2% steel fibers by volume. Four girders measured 9.75 m in length and 0.90 m in height, while two measured 11.60 m in length, and 1.10 m in height. The research program considered a range of variables significant to the shear design of UHPC bridge girders, including UHPC with different mechanical properties, girder height (0.90–1.10 m), web width (0.08–0.10 m), bottom prestressing area ($A_{p_{bot}}$) (0–4522 mm^2), and the incorporation of vertical steel reinforcement in the web (0.00%–1.29%). The study aimed to understand the influences of these variables on UHPC girder performance under shear loading. A summary of the specimens analyzed as part of this validation study is provided in Table 4. The failure mechanism of the beams was characterized by the propagation of cracks in the shear-critical region followed by the formation of a critical shear crack prompting the shear failure. The crack patterns for each specimen are provided in Figure 10a.

Uniaxial compression and direct tension tests were conducted as material characterization tests. These results were used in the FE model to validate its accuracy in predicting the response of UHPC beams when

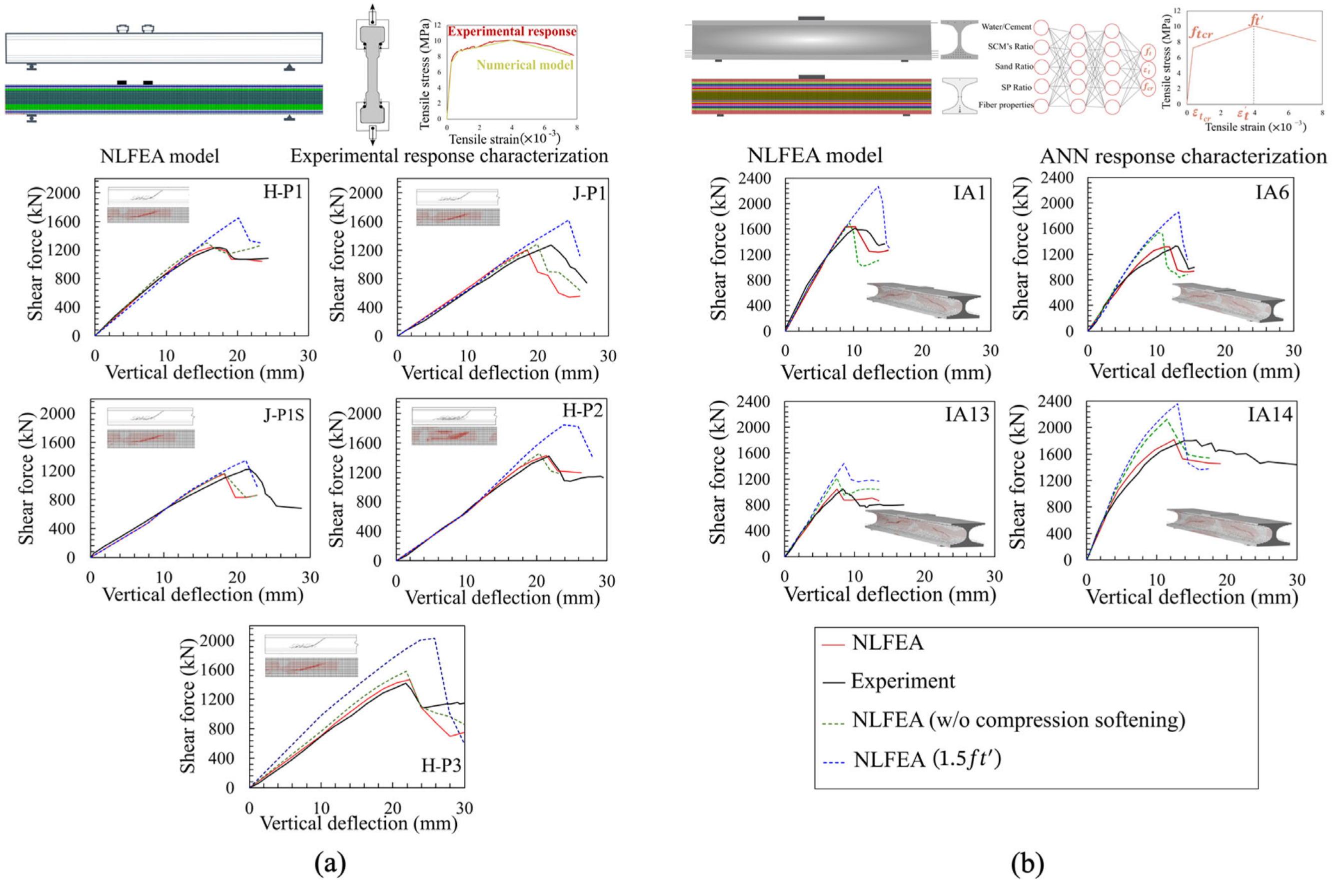

FIGURE 10 Modeling illustration and experimental versus analytical results of the UHPC beams using (a) experimental response characterization for UHPC tension response[32] and (b) ANN response characterization for UHPC tension response.[4]

experimental data for UHPC uniaxial tension response characterization is available from material testing.

The beams were modeled using a combination of rectangular membrane elements representing the UHPC and truss bar elements representing the prestressing reinforcement, as shown in Figure 10a. The model contained 3900–4095 rectangular elements, 390 truss bar elements, and 4116–4132 nodes, the numbers varying based on the dimensions of the modeled beams. The mesh size was selected based on dividing the height of the beam by 10–15 elements and keeping the element height-toto-width ratio approximately equal to 1.0 based on previously proven mesh size adequacy.[64] The boundary conditions, including the support conditions and the loading plates, were chosen to replicate the experimental support conditions. The duration of a typical analysis was approximately 2 min. The NLFEA showed accurate results in terms of the load-deflection behavior, failure mechanism, and the crack pattern when compared with the experimental results, as shown in Figure 10a. A sensitivity analysis was conducted on the effect of the direct tensile strength and the compression softening on the modeling accuracy by analyzing the beams with 1.5 times the reported direct tensile strength and without the proposed compression softening model. The choice for changing the tensile strength emerged from the high variability in the measured direct tensile strength of UHPC mixes, unlike their compressive strengths, sometimes by even more than 50% for the same mix. The results show that the direct tensile strength had a higher effect on the behavior of the modeled beams, whereas the compression softening had a relatively lower effect on the modeling results compared to the direct tensile strength, as it mainly affected the post-peak behavior of the modeled UHPC beams, as shown in Figure 10a. However, the compression softening effect can be more pronounced in other structural members where the axial loads are relatively higher, such as UHPC shear walls.

4.3 | Beam specimens—Phase III

The final phase in this validation study consisted of modeling beam specimens that did not provide UHPC mechanical properties from direct tension tests. The UHPC beam specimens selected for validation were

TABLE 5 Properties of the eCPCI tested specimens.[4]

ID	f'_c MPa	f'^{a}_t MPa	f^{a}_{cr} MPa	ε'^{a}_t $\times 10^{-3}$	$A_{p_{bot}}$ mm^2	$A_{s_{bot}}$ mm^2	b_w mm	a/d -
IA1	155	12.8	7.3	5.0	4592	0	76	2.5
IA6	122	12.0	5.3	4.2	2296	4644	76	2.5
IA13	126	12.0	5.3	4.2	4592	0	51	2.5
IA14	126	12.0	5.3	4.2	4592	0	102	2.5

Note: f'_c: UHPC compressive strength; f'^{a}_t: UHPC tensile strength (values were calculated using the developed ANN model); f^{a}_{cr}: UHPC cracking stress (values were calculated using the developed ANN model); ε'^{a}_t: UHPC strain at peak tensile strength (values were calculated using the developed ANN model); $A_{p_{bot}}$: prestressed steel reinforcement area; $A_{s_{bot}}$: conventional steel reinforcement area; a/d: shear-span-to-depth ratio.

tested by the Wiss, Janney, Elstner (WJE) engineering firm in association with the Precast, Pretensioned Concrete Institute (PCI) under a collaboration project involving e.Construct and PCI (eCPCI).[4] The study aimed to assess the effect of different parameters on the shear behavior of UHPC beams. The UHPC beams were constructed with a novel cross-sectional profile, as shown in Figure 10b, to optimize their structural behavior.

The experimental program involved testing to failure of 16 shear-critical UHPC beams. This study focused on modeling beams that had an a/d ratio higher than two and that had no transverse reinforcement. The test variables included the effect of thermal treatment, replacement of prestressing reinforcement with conventional ribbed steel bar reinforcement, fiber reinforcement characteristics, a/d ratio, transverse reinforcement ratio, web widths, and beam height. A summary of the mechanical properties of the selected beams for this validation study is provided in Table 5. The modeled beams had a length of 5.5 m and a height of 0.86 m and investigated the effect of the web width, and the replacement of prestressed reinforcement, $A_{p_{bot}}$, with non-prestressed reinforcement, $A_{s_{bot}}$, on the shear behavior of UHPC beams, as shown in Table 5. The failure of the beams was characterized mainly by the formation of a diagonal tension crack in the web followed immediately by concrete compression failure.

The cross section was modeled by varying the thickness of the element's layers through the depth of the beams, as shown in Figure 10b. The finite element model consisted of 8428 rectangular elements, 690 truss elements, and 9639 nodes. Half of the beam was modeled due to the symmetry of the tests. The analyses accurately captured the behavior of the UHPC beams, as shown in Figure 10b.

A sensitivity analysis was conducted similar to the one in Phase II; the sensitivity analysis results show the pronounced effect of the direct tensile strength on the shear behavior of the modeled beams. Nevertheless, the compression softening also had a noticeable effect on the shear behavior of the modeled beams. This is due to the relatively high compressive stresses present in the critical shear regions of these beams from the prestressing strands located near the web region, as shown in Figure 10b.

The results of the NLFEA were accurate in depicting the shear behavior of the beams, as shown in Figure 10a,b. The NLFEA was then further validated by testing other UHPC beams provided in the literature. The modeling results were accurate in estimating the shear capacities of the UHPC beams compared to the experimental results, a general overview of the beams in addition to a comparison between the modeling and experimental results in terms of the shear capacity are provided in Table A1 in Appendix A.

5 | CONCLUSIONS

This study introduces an ANN model combined with NLFEA for assessing the response of UHPC shear-critical structural members. The following conclusions can be made:

1. Smeared hybrid rotating crack formulations, such as the DSFM,[28] are valid platforms for the analysis of UHPC members at the macro-scale. For the realistic representation of UHPC member behavior, it is important for the formulation employed to allow for slip along the crack interfaces, divergence of the stress and strain fields, as well as rotation of the crack direction, consistent with experimental observations.
2. The characterization of the uniaxial direct tension behavior of UHPC is critical for modeling the response of UHPC members. This behavior is significantly influenced by the mix design constituents and the physical properties of the fiber reinforcement. Employing an ANN to output the mechanical properties of the UHPC in tension was shown to be advantageous for NLFEA.

3. The SHAP analysis results for the developed ANN show that while the fiber reinforcement characteristics have a relatively pronounced impact on the direct tension strength of UHPC, other parameters including the W/C ratio, SCM ratio, and sand-to-cement ratio are also influential. This comprehensive understanding is essential for refining UHPC tension models and ensuring their robustness and accuracy.
4. The UHPC biaxial compressive strength is modified to account for the softening behavior under transverse tensile strains and associated cracking. The tensile stress–strain model used in the analysis was found to significantly influence the ultimate shear capacity of UHPC beams. The compression softening model was found to have a less pronounced effect on the shear behavior of the modeled beams, depending on the magnitude of the compressive stresses present in the critical shear region.
5. The straining at crack locations observed in the UHPC beams analyzed in this study including the beams tested by El-Helou and Graybeal[32] and eCPCI[4] compromises the post-cracking ductility and shear transfer capacity. This called for the use of a crack width limit which better simulates the actual behavior of UHPC members.
6. The NLFEA implementation conveyed accurate results in simulating the behavior of UHPC members using either the uniaxial direct tension results or the ANN predicted tensile results.

6 | FUTURE WORK

Future efforts will focus on developing a fiber orientation model for UHPC members based on their casting method and cross-sectional dimensions. Ultimately, the authors aim to establish practical guidelines using this model for optimizing the structural performance of UHPC members in engineering applications.

ACKNOWLEDGMENTS

The authors acknowledge the Daniel P. Jenny Research Fellowship Program of the Precast/Prestressed Concrete Institute (PCI) for providing funding for this research.

DATA AVAILABILITY STATEMENT

The data that support the findings of this study are available from the corresponding author upon reasonable request.

REFERENCES

1. Bajaber MA, Hakeem IY. UHPC evolution, development, and utilization in construction: a review. J Mater Res Technol. 2021;10:1058–74. https://doi.org/10.1016/j.jmrt.2020.12.051
2. Amran M, Huang SS, Onaizi AM, Makul N, Abdelgader HS, Ozbakkaloglu T. Recent trends in ultra-high performance concrete (UHPC): current status, challenges, and future prospects. Construct Build Mater. 2022;352:129029. https://doi.org/10.1016/J.CONBUILDMAT.2022.129029
3. Zhang G, Graybeal BA. Development of UHPC pi-girder sections for span length up to 41 m. J. Bridge Eng. 2015;20(3):04014068.
4. Tadros M, Lawler J, El-Khier M, Gee D, Kurt A, Lucier G, et al. Implementation of Ultra-High Performance Concrete in Long-Span Precast Pretensioned Elements for Concrete Buildings and Bridges. 2021.
5. Lv Y, Qin Y, Wang J, Li G, Zhang P, Liao D, et al. Effect of incorporating hematite on the properties of ultra-high performance concrete including nuclear radiation resistance. Construct Build Mater. 2022;327:126950. https://doi.org/10.1016/J.CONBUILDMAT.2022.126950
6. Milasi SE, Mostofinejad D, Bahmani H. Improving the resistance of ultra-high-performance concrete against nuclear radiation: replacing cement with barite, hematite, and lead powder. Develop Built Environ. 2023;15:100190. https://doi.org/10.1016/J.DIBE.2023.100190
7. Khan MU, Ahmad S, Naqvi AA, Al-Gahtani HJ. Shielding performance of heavy-weight ultra-high-performance concrete against nuclear radiation. Prog Nucl Energy. 2020;130:103550. https://doi.org/10.1016/J.PNUCENE.2020.103550
8. Caruso MC, Pascale C, Camacho E, Ferrara L. Comparative environmental and social life cycle assessments of off-shore aquaculture rafts made in ultra-high performance concrete (UHPC). Int J Life Cycle Assess. 2022;27:281–300. https://doi.org/10.1007/s11367-021-02017-6
9. Lin Y, Yan J, Wang Z, Zou C. Effects of steel fibers on failure mechanism of S-UHPC composite beams applied in the Arctic offshore structure. Ocean Eng. 2021;234:109302. https://doi.org/10.1016/j.oceaneng.2021.109302
10. Bencardino F, Rizzuti L, Spadea G, Swamy RN. Stress-strain behavior of steel fiber-reinforced concrete in compression. J Mater Civil Eng. 2008;20:255–63. https://doi.org/10.1061/(ASCE)0899-1561(2008)20:3(255)
11. Moradi M, Bagherieh AR, Esfahani MR. Constitutive modeling of steel fiber-reinforced concrete. Int J Damage Mech. 2020;29:388–412. https://doi.org/10.1177/1056789519851159
12. Schauffert EA, Cusatis G. Lattice discrete particle model for fiber-reinforced concrete. I: theory. J Eng Mech. 2012;138:826–33. https://doi.org/10.1061/(ASCE)EM.1943-7889.0000387
13. Zhang J, Wu Z, Yu H, Ma H, Da B. Mesoscopic modeling approach and application for steel fiber reinforced concrete under dynamic loading: a review. Engineering. 2022;16:220–38. https://doi.org/10.1016/j.eng.2022.01.011
14. Lee SC, Cho JY, Vecchio FJ. Diverse embedment model for steel fiber-reinforced concrete in tension: model verification. ACI Mater. J. 2011;108(5):526–35.
15. Voo JYL, Foster SJ. Variable engagement model for the design of fibre reinforced concrete structures. Advanced materials for construction of bridges, buildings, and other structures III. Proc. advanced materials for construction of bridges, buildings, and other structures iii engineering conferences international year 2003. Davos, Switzerland; 2003.

16. Lakavath C, Prakash SS. Influence of fiber dosage, fiber type, and level of prestressing on the shear behaviour of UHPFRC I-girders. Eng Struct. 2024;300:117146. https://doi.org/10.1016/j.engstruct.2023.117146
17. El-Helou RG, Graybeal BA. Shear design of strain-hardening fiber-reinforced concrete beams. J Struct Eng. 2023;149:1–16. https://doi.org/10.1061/jsendh.steng-11065
18. Ross B, Tarawneh A, Naser M, Ferche A, Diab A. Comparison of recent shear capacity models against experimental and simulation databases of prestressed UHPC beams. PCI J. 2024; 37–57.
19. Padmarajaiah SK, Ramaswamy A. A finite element assessment of flexural strength of prestressed concrete beams with fiber reinforcement. Cem Concr Compos. 2002;24:229–41. https://doi.org/10.1016/S0958-9465(01)00040-3
20. Manzoli OL, Oliver J, Huespe AE, Diaz G. A mixture theory based method for three-dimensional modeling of reinforced concrete members with embedded crack finite elements. Comput Concrete. 2008;5:401–16. https://doi.org/10.12989/cac.2008.5.4.401
21. Vrech S, Etse G, Caggiano A. Thermodynamically consistent elasto-plastic microplane formulation for fiber reinforced concrete. Int J Solid Struct. 2016;81:337–49. https://doi.org/10.1016/J.IJSOLSTR.2015.12.007
22. Bi J, Huo L, Zhao Y, Qiao H. Modified the smeared crack constitutive model of fiber reinforced concrete under uniaxial loading. Construct Build Mater. 2020;250:118916. https://doi.org/10.1016/j.conbuildmat.2020.118916
23. Bai W, Lu X, Guan J, Huang S, Yuan C, Xu C. Stress–strain behavior of FRC in uniaxial tension based on mesoscopic damage model. Cryst. 2021;11:689. https://doi.org/10.3390/cryst11060689
24. Fu Q, Bu M, Xu W, Chen L, Li D, He J, et al. Comparative analysis of dynamic constitutive response of hybrid fibre-reinforced concrete with different matrix strengths. Int J Impact Eng. 2021;148:103763. https://doi.org/10.1016/j.ijimpeng.2020.103763
25. Denneman E, Kearsley EP, Visser AT. Splitting tensile test for fibre reinforced concrete. Mater Struct. 2011;44:1441–9. https://doi.org/10.1617/s11527-011-9709-x
26. Diab A, Ferche A. Prediction of the tensile properties of UHPC using artificial neural network. ACI Struct J. 2023;121:57–69. https://doi.org/10.14359/51740245
27. Wong PS, Vecchio FJ, Trommels H. Vector2 & formworks user's manual. second ed. Canada: University of Toronto; 2013.
28. Vecchio FJ. Disturbed stress field model for reinforced concrete: formulation. J Struct Eng. 2000;126:1070–7.
29. Yap B. Behaviour of ultra high performance fibre reinforced concrete subjected to pure shear. 2020. Available from: http://ezproxy.lib.utexas.edu/login?url=https://www.proquest.com/dissertations-theses/behaviour-ultra-high-performance-fibre-reinforced/docview/2425651578/se-2?accountid=7118
30. Hasgul U, Yavas A, Birol T, Turker K. Steel fiber use as shear reinforcement on I-shaped UHP-FRC beams. Appl Sci. 2019;9. https://doi.org/10.3390/app9245526
31. Baby F, Marchand P, Toutlemonde F. Shear behavior of ultra-high performance fiber-reinforced concrete beams. I: experimental investigation. J Struct Eng. 2014;140. https://doi.org/10.1061/(ASCE)ST.1943-541X.0000907
32. El-Helou RG, Graybeal BA. Shear behavior of ultrahigh-performance concrete pretensioned bridge girders. J Struct Eng. 2022;148. https://doi.org/10.1061/(asce)st.1943-541x.0003279
33. Voo YL, Poon WK, Foster SJ. Shear strength of steel fiber-reinforced ultrahigh- performance concrete beams without stirrups. J Struct Eng. 2010;136:1393–400. https://doi.org/10.1061/(ASCE)ST.1943-541X.0000234
34. Said A, Elmorsi M, Nehdi M. Non-linear model for reinforced concrete under cyclic loading. Magazine Concr Res. 2005;57: 211–24.
35. Sittipunt C, Wood SL. Influence of web reinforcement on the cyclic response of structural walls. J. Struct. 1995;92(6):745–56.
36. Hu HT, Schnobrich WC. Nonlinear analysis of cracked reinforced concrete. ACI Struct. J. 1990;87(2):199–207.
37. Broujerdian V. Smeared rotating crack model for reinforced concrete membrane elements. ACI Struct J. 2010;107:411–8. Available from: https://www.researchgate.net/publication/287695099
38. Foster SJ, Budiono B, Gilbert RI. Rotating crack finite element model for reinforced concrete structures. Comput Struct. 1996; 58:43–50. https://doi.org/10.1016/0045-7949(95)00109-T
39. Vecchio FJ, Collins MP. The modified compression-field theory for reinforced concrete elements subjected to shear. ACI Struct J. 1986;83:219–31.
40. Hung C-CH, El-Tawil S. Hybrid rotating/fixed-crack model for high-performance fiber-reinforced cementitious composites. ACI Mater J. 2010;107:568–76.
41. Bažant ZP, Xiang Y, Prat PC. Microplane model for concrete. I: stress-strain boundaries and finite strain. J Eng Mech. 1996; 122:245–54. https://doi.org/10.1061/(ASCE)0733-9399(1996)122:3(245)
42. Ožbolt J, Li Y, Kožar I. Microplane model for concrete with relaxed kinematic constraint. Int J Solid Struct. 2001;38:2683–711. https://doi.org/10.1016/S0020-7683(00)00177-3
43. Cusatis G, Mencarelli A, Pelessone D, Baylot J. Lattice discrete particle model (LDPM) for failure behavior of concrete. II: calibration and validation. Cem Concr Compos. 2011;33:891–905. https://doi.org/10.1016/J.CEMCONCOMP.2011.02.010
44. Jin C, Buratti N, Stacchini M, Savoia M, Cusatis G. Lattice discrete particle modeling of fiber reinforced concrete: experiments and simulations. Eur J Mech A Solids. 2016;57:85–107. https://doi.org/10.1016/J.EUROMECHSOL.2015.12.002
45. Vecchio FJ. Towards cyclic load modeling of reinforced concrete. ACI Struct. J. 1999;96:193–202.
46. Mészöly T, Randl N. Shear behavior of fiber-reinforced ultra-high performance concrete beams. Eng Struct. 2018;168:119–27. https://doi.org/10.1016/j.engstruct.2018.04.075
47. Franssen R, Guner S, Courard L, Mihaylov BI. Numerical modeling approach for UHPFRC members including crack spacing formulations. Eng Struct. 2021;238:112179. https://doi.org/10.1016/j.engstruct.2021.112179
48. Lim W-Y, Hong S-G. Shear tests for ultra-high performance fiber reinforced concrete (UHPFRC) beams with shear reinforcement. Int J Concr Struct Mater. 2016;10:177–88. https://doi.org/10.1007/s40069-016-0145-8
49. Reinhardt HW, Walraven JC. Cracks in concrete subject to shear. J Struct Div. 1982;108:207–24. https://doi.org/10.1061/JSDEAG.0005860

50. Graybeal B, Davis M. Cylinder or cube: strength testing of 80 to 200 MPa (11.6 to 29 ksi) ultra-high-performance fiber-reinforced concrete. ACI Mater. J. 2008;105(6):603.
51. El-Helou RG, Haber ZB, Graybeal BA. Mechanical behavior and design properties of ultra-high-performance concrete. ACI Mater J. 2022;119:181–94. https://doi.org/10.14359/51734194
52. Abellán-García J. Four-layer perceptron approach for strength prediction of UHPC. Construct Build Mater. 2020;256:119465. https://doi.org/10.1016/j.conbuildmat.2020.119465
53. Hoshikuma J, Kawashima K, Nagaya K, Taylor AW. Stress-strain model for confined reinforced concrete in bridge piers. J Struct Eng. 1997;123:624–33. https://doi.org/10.1061/(ASCE)0733-9445(1997)123:5(624)
54. Lee J-H, Hong S-G, Joh C, Kwahk I, Lee J-W. Biaxial tension–compression strength behaviour of UHPFRC in-plane elements. Mater Struct. 2017;50:20. https://doi.org/10.1617/s11527-016-0918-1
55. Kupfer H, Hilsdorf HK, Rusch H. Behavior of concrete under biaxial stresses. J. proc. 1969;66(8):656–66.
56. Fehling E, Leutbecher T, Röder FK, Stürwald S. Structural behavior of UHPC under biaxial loading. Ultra High Performance Concrete (UHPC). 2008;2:05–7.
57. Leutbecher T. Structural behavior of ultra-high performance (fiber-reinforced) concrete compression struts subjected to transverse tension and cracking. Struct Concr. 2020;21:2154–67. https://doi.org/10.1002/suco.201900451
58. Liu R-R, Ding R, Fan J-S, Tao M-X. Constitutive laws of softened UHPC in biaxial tension–compression: experimental study using a planar bi-directional element tester. Construct Build Mater. 2023;401:132966. https://doi.org/10.1016/j.conbuildmat.2023.132966
59. Lee S-C, Cho J-Y, Vecchio FJ. Simplified diverse embedment model for steel fiber reinforced concrete elements in tension. ACI Mater J. 2013;110:403–12.
60. Zhang H, Huang YJ, Yang ZJ, Xu SL, Chen XW. A discrete-continuum coupled finite element modelling approach for fibre reinforced concrete. Cem Concr Res. 2018;106:130–43. https://doi.org/10.1016/j.cemconres.2018.01.010
61. Diab A, Ferche A. UHPC direct tension database. 2024. Available from: https://www.kaggle.com/dsv/7869505
62. Qi J, Ding X, Wang Z, Hu Y. Shear strength of fiber-reinforced high-strength steel ultra-high-performance concrete beams based on refined calculation of compression zone depth considering concrete tension. Adv Struct Eng. 2019;22:2006–18. https://doi.org/10.1177/1369433219829805
63. Yang I-H, Joh C, Kim B-S. Shear behaviour of ultra-high-performance fibre-reinforced concrete beams without stirrups. Magazine Concr Res. 2012;64:979–93. https://doi.org/10.1680/macr.11.00153
64. Saatci S, Vecchio FJ. Nonlinear finite element modeling of reinforced concrete structures under impact loads. ACI Struct J. 2009;106:717–25.
65. Voo JYL. An investigation into the behaviour of prestressed reactive powder concrete girders subject to non-flexural actions (Doctoral dissertation, UNSW Sydney). UNSW University; 2004 Doctoral Dissertation.
66. Ueda M, Noguchi H, Shirai N, Morita S. Introduction to activity of new RC. Proc. Int. workshop on finite element analysis of reinforced concrete. Proc. Int. workshop on finite element analysis of reinforced concrete. New York, N.Y.: Columbia University; 1991.

AUTHOR BIOGRAPHIES

Amjad Diab is a PhD student at the Maseeh Department of Civil, Architectural and Environmental Engineering, The University of Texas at Austin. His research interests include performance assessment and analysis of concrete structures, structural implications of deterioration mechanisms, and sustainability of concrete structures. Department of Civil, Architectural and Environmental Engineering, The University of Texas at Austin, Austin, Texas, USA. Email: amjad.diab@utexas.edu

Anca Ferche is an Assistant Professor in the Maseeh Department of Civil, Architectural and Environmental Engineering, The University of Texas at Austin, TX. Her research interests include performance assessment and analysis of reinforced concrete structures, concrete deterioration mechanisms, and rehabilitation of structures. Department of Civil, Architectural and Environmental Engineering, The University of Texas at Austin, Austin, Texas, USA. Email: ferche@austin.utexas.edu

How to cite this article: Diab A, Ferche A. Modeling the response of UHPC shear-critical beams: Integrating nonlinear finite element analysis and artificial neural network. Structural Concrete. 2025. https://doi.org/10.1002/suco.70191

APPENDIX A

TABLE A1 Comparative analysis of shear capacity modeling results of UHPC beams.

		b_W (mm)	h (mm)	A/D	$A_{P_{bot}}$ (mm^2)	$A_{S_{bot}}$ (mm^2)	V_{exp} (KN)	$V_{calc.}$ (KN)	$\frac{V_{exp}}{V_{calc}}$
65	SB1	50	650	3.0	1716	0	430	410	0.95
	SB2	50	650	3.0	1716	0	497	490	0.99
	SB3	50	650	3.0	1716	0	428	422	0.99
	SB4	50	650	3.0	1716	0	337	364	1.08
	SB5	50	650	3.0	1716	0	440	449	1.02
	SB6	50	650	3.0	1716	0	330	325	0.98
	SB7	50	650	3.0	1716	0	400	434	1.09
33	X-B1	50	650	3.2	1200	0	330	350	1.06
	X-B2	50	650	3.2	1200	0	355	363	1.02
	X-B3	50	650	3.2	1200	0	360	395	1.10
	X-B4	50	650	2.5	1200	0	456	466	1.02
	X-B5	50	650	3.5	1200	0	423	432	1.02
	X-B6	50	650	4.5	1200	0	391	357	0.91
	X-B7	50	650	2.5	1200	0	522	604	1.16
	X-B8	50	650	1.8	1200	0	582	604	1.04
31	UHPFRC-A-PC-NS	65	380	2	900	0	430	511	1.19
	UHPFRC-A-PC-NS2	65	380	2	900	0	431	511	1.18
	UHPFRC-B-PC-NS	65	380	2	900	0	507	510	1.00
	UHPFRC-A-RC-NS	65	380	2	0	2061	454.5	423	0.93
	UHPFRC-B-RC-NS	65	380	2	0	2061	447.5	424	0.95
	UHPC-A-NF-RC-NS	65	380	2	0	2061	180.5	163	0.90
30	NF	100	150	4	0	628	35.6	37	1.04
	S6 (0.5)	100	150	4	0	628	40.65	55	1.35
	S6 (1.0)	100	150	4	0	628	59.08	57	0.96
	S6 (1.5)	100	150	4	0	628	55.58	59	1.05
	S13 (0.5)	100	150	4	0	628	56.19	58	1.02
	S13 (1.0)	100	150	4	0	628	63.49	60	0.95
	H30 (0.5)	100	150	4	0	628	40.58	63	1.56
	H30 (1)	100	150	4	0	628	61.5	58	0.93
	H30 (1.5)	100	150	4	0	628	71.74	60	0.83
	H60 (0.5)	100	150	4	0	628	36.21	37	1.03
	H60 (1)	100	150	4	0	628	48.58	51	1.05
	H60 (1.5)	100	150	4	0	628	57.89	58	1.00
						Average $\frac{V_{exp}}{V_{calc}}$			1.04
						C.O.V			0.13